Article

Performance of Alternative Methane Reforms Based on Experimental Kinetic Evaluation and Simulation in a Fixed Bed Reactor

Augusto Knoelchemann [1], Deivson C. S. Sales [2], Marcos A. M. Silva [1] and Cesar A. M. Abreu [1,*]

[1] Department of Chemical Engineering, Federal University of Pernambuco, Recife 50.740-521, Brazil; augustokn9@yahoo.com.br (A.K.); mamsilva2004@yahoo.com.br (M.A.M.S.)

[2] Polytechnic School, State University of Pernambuco, Recife 50.740-521, Brazil; deivsonsales@poli.br

* Correspondence: cesar@ufpe.br; Tel.: +55-81-21268238

Abstract: A comparative evaluation of alternative methane reforming processes as an option to steam reforming was performed by carrying out simulations of operations in a fixed bed reactor with a Ni (4.8 wt.%/γ-Al$_2$O$_3$) catalyst at 1023 K under 1.0 bar. Methane reforms, including processing with carbon dioxide (DRM, CH$_4$/CO$_2$), autothermal reform (ATRM, CH$_4$/H$_2$O/O$_2$), and combined reform (CRM, CH$_4$/CO$_2$/H$_2$O/O$_2$) had their operations predicted based on experimental data developed to represent their kinetic behavior, formalized with mechanisms and parametric quantifications. The performance of fixed bed reactor operations for methane conversions occurred with different reaction rates in the three alternative processes, and comparatively the orders of magnitude were 10^2, 10^{-1}, and 10^{-4} in CRM, ATRM, and DRM, respectively. According to each process, the methane conversions were oriented towards the predominant productions of hydrogen or carbon monoxide, indicating the kinetic selectivities of H$_2$, 86.1% and CO, 59.2% in CRM and DRM, respectively. Considering the possibility of catalyst deactivation by carbon deposition, its predicted yields are low due to the slow stages of its production and due to its simultaneous consumption through interactions with O$_2$, CO$_2$, and H$_2$O, reflecting favorably in additional productions of H$_2$ and CO.

Keywords: methane; alternative reforms; kinetic; fixed bed; comparative; performance

1. Introduction

Different reform technologies' studies and their combinations converge on the production of different intermediate chemicals or final products such as hydrocarbons, methanol, natural gasoline, and diesel oil [1–4]. Methane steam reform, due to its characteristics, is the process most employed to convert natural gas into synthesis gas to meet the demand for synthetic liquid fuels via GTL (gas–to–liquids) technologies. Advantageously, this route produces a synthesis gas with high H$_2$/CO ratios (3:1), indicated as feed for ammonia synthesis processes, oil refining (hydrotreating, hydrocracking, etc.), and hydrocarbon synthesis via Fischer–Tropsch, in addition to the hydrogen production itself.

Alternatively, using other types of methane reforms, different synthesis gases can be obtained, meaning several intermediate products must attend to the subsequent production of various derivatives. Reforms other than steam reforming, here called alternatives, have the potential to produce synthesis gas with different compositions in terms of the H$_2$/CO ratio.

For each of these processes, aspects that impact its performance can be highlighted. Reactions with H$_2$O, CO$_2$, and O$_2$, characterizing the SRM, DRM, and POM reforms, respectively, may present advantages and disadvantages related mainly to the reaction kinetics and thermality, coke deposition, and intrinsic catalyst regeneration.

In order to operate the methane conversion with the best performance, the objective is to combine the advantages of each of the reforms and reduce their disadvantages. Thus, steam reforming and carbon dioxide reforming, combining with other reforms, includ-

ing autothermal reforming and partial oxidation, can provide possibilities for achieving significant performances.

In this context are included the dry reform with carbon dioxide (DRM), the autothermal reform of methane with oxygen and water (ATRM), and the combined reform of methane with three components with oxygen, water, and carbon dioxide (CRM) [5–7].

DRM is an endothermic process, requiring large amounts of energy, and providing a H_2/CO ratio at the level of one unit. ATR combines endothermic steam reforming with partial exothermic oxidation reactions leading to different H_2/CO ratios and has low energy requirements. The association of the dry reform with the stages of steam reform and the partial oxidation of methane constitutes low thermality CRM.

The dry methane reform was carried out employing different catalysts. However, efforts have been made to continue the effective use of nickel catalysts [8]. Thus, the production of the synthesis gas was carried out with Ni-catalysts, optimizing their performance by varying the parameters such as the type of support, promoters, and the synthesis of the catalyst. Employed to the DRM, Ni–Mo nanocatalysts resistant to coke and sintering were synthesized as a molybdenum-doped nickel with monocrystalline MgO [9]. Experiments on the autothermal reform of methane were carried out for operations with structured Si−SiC catalysts based on Ni–Rh, and mechanisms were formulated to be used in the modeling of the process [10]. Kinetic studies were performed varying the input concentration of methane, water, and carbon dioxide. Other theoretical studies were used as a basis for establishing a mechanism for ATR [11]. An adequate syngas (H_2/CO) was produced by performing the TRM with adjusted operating variables (GHSV, feed composition), providing a long reaction time under low coke deposition [12].

For the Fischer–Tropsch synthesis, CRM was performed using nickel supported on $MgAl_2O_4$ promoted with Zr, Ce, and Ce–Zr [13]. These systems were effective to prevent nickel oxidation and deactivation by carbon deposition. In order to intensify the production of a more suitable syngas for the employment of CRM, an alternative was recently proposed through the combination of steam and dry reformings [14].

Conventional operations of industrial natural gas reform processes use catalytic fixed bed reactors, which are subjected to high temperature conditions under different pressure ranges and involve mass transfer and thermal non-uniformity effects. Thus, this equipment operates in different kinetic regimes (chemical, intermediate, diffusive), presenting operational requirements that guarantee conversions and yields appropriate to industrial practice. The operation times count on the active life of the catalyst where its deactivation (coke, sintering, etc.) must be under constant observation.

Due to the effect on methane stability by the use of new catalysts and equipments improving its conversion, the development of different reform technologies are in perspective. In the present approach, based on proposals for mechanisms and quantifications of the kinetics of alternative reforms [5–7] conducted by our research group, their operations were simulated in a fixed bed reactor in the presence of a supported nickel catalyst on alumina. Data obtained in our reseach were applied as the basis for each of the processes, and included the mass balance formulations for the fixed bed reactor. The results were compared in terms of the evolution and concentration profiles of hydrogen and carbon monoxide produced, as well as the carbon content with potential for deposition and consequent deactivation of the catalyst. The formulated predictions were confirmed as effective for comparing the performances of the three methane reforms.

2. Materials and Methods

For the purpose of conducting a comparative assessment between alternative methane reform processes, other than steam reform, a numerical simulation of their operations in a fixed bed reactor was employed. For this, the following strategy was adopted: identification and characterization of the catalyst used in the kinetic evaluations of the reform processes; formulation of the mass balances of the components of each process for isothermal operations and inclusion of the expressions of apparent reaction rates; consideration of the gas

flow with axial dispersion; consideration of the kinetics of reactions without limitations due to the effects of mass transfer; use of quantified reaction rates with experimental bases.

The nickel catalyst with an estimated metal content of 5.0% by weight was prepared from its salt precursor via the incipient wetting method involving impregnation, calcination, and reduction. Material characteristics were obtained by AAS (atomic absorption spectrometry), XRD (X-ray diffraction, XRD, CuK–alpha radiation), and textural analysis (BET–N_2 method).

For the kinetic operational evaluations of each process, a small-scale fixed bed reactor was used (2.0 g cat., <dp> = 50 μm) operating isothermally at 1023 K under atmospheric pressure ([5–7]). Different gas feed compositions were used according to the reforming process, and with each composition different flow rates were practiced, meaning variations in space time. Under each feed composition and applying different flow rates, a steady state was established for each one of them, observed by the constant composition of the reactor effluent product.

The experimental data obtained in the spatial time domain served to validate the proposed reaction rate expressions for each component in each process and allowed the estimation of the orders of magnitude of the kinetic parameters.

Predicting the methane behavior in the reforms in a fixed bed reactor on a pilot scale, mass balances were formulated for the components of each process, which included the validated reaction rates. The solutions of the balance equations led to the predictions of operation behavior through concentration profiles.

The simulations indicated by the experimental bases involved in them, characterized the comparisons of the alternative reforms in terms of the yields in hydrogen and carbon monoxide, and in relation to the production of carbon.

2.1. Numerical Method

The simulation of the operational behavior of the reform processes was carried out through the solutions of the partial differential equations formulated by the mass balances related to the chemical components involved. The method of solving the model of equations for methane reforms involved discretization in terms of time and space. Second-order spatial discretization was applied in relation to position, while a method based on numerical differentiation (numerical differentiation formulas, NDFs) provided solutions for concentration over time. The solutions of the model equations (Equation (18)), associated with the initial conditions and the boundary conditions (Equation (19)), were elaborated by applying the line method, recurring to the spatial and temporal discretization, where the space dependent variables ($\Delta x = L/[n - 1]$) and time ($\Delta t = tn[nt - 1]^{-1}$) were the object of simultaneous interactions. For each advance of the concentration in time, the calculation of the concentration profiles followed, continuing until all the pre-established points in time (nt) were covered. Numerical differentiation (NDFs) was employed to obtain the evolution based on the expansion of the various derivatives in the Taylor series, in terms of the central point. An algorithm was formulated serving the calculation by the line method. The discretization for evaluations in space is expressed as:

$$\frac{\partial^2 C}{\partial x^2} = \frac{C_{i,k-1} - 2C_{i,k} + C_{i,k+1}}{\Delta x^2}, \ \frac{\partial C}{\partial x} = \frac{C_{i,k} - C_{i,k-1}}{\Delta x} \tag{1}$$

To calculate the concentration over time,

$$C_i(t_0 + \Delta t) = C_i(t_0) + \Delta t \frac{dC_i(t_0)}{dt} + \frac{1}{2}\Delta t^2 \frac{d^2C_i(t_0)}{dt^2} + \frac{1}{6}\Delta t^3 \frac{d^3C_i(t_0)}{dt^3} + \frac{1}{24}\Delta t^4 \frac{d^4C_i(t_0)}{dt^4} \tag{2}$$

$$C_i(t_0 - \Delta t) = C_i(t_0) - \Delta t \frac{dC_i(t_0)}{dt} + \frac{1}{2}\Delta t^2 \frac{d^2C_i(t_0)}{dt^2} - \frac{1}{6}\Delta t^3 \frac{d^3C_i(t_0)}{dt^3} + \frac{1}{24}\Delta t^4 \frac{d^4C_i(t_0)}{dt^4} \tag{3}$$

$$\frac{dC_i(t_0)}{dt} = -\frac{3C_i(t_0 - \Delta t) - 3C_i(t_0 + \Delta t) + \Delta t^3 \frac{d^3C_i(t_0)}{dt^3}}{6\Delta t} \tag{4}$$

From the discretization of the system of differential equations, it was possible to obtain the evolution and the concentration profiles of the reagents and products present in the reaction medium of the reform processes in operation in the fixed bed reactor.

3. Kinetics and Reactor Modeling

The experimental bases for methane reform processes were developed in our previous studies [5–7] via a kinetic approach, referring to the DRM methane dry reform of methane [5], the ATRM autothermal reform of methane [6], and the CRM combined methane reform [7]. In sequence, the reform processes, their reaction steps (*i*) and the corresponding reaction rates (r_i) are described.

3.1. Kinetics of Reforming Processes

The kinetic behavior of the reform processes were previously evaluated from the experimental data of the proposed reaction rates formulated for the steps of each process. The expressions of these rates, containing the respective quantified parameters, were included in the mass balances of the fixed bed reactor used to simulate the operations of the methane reforms.

Dry methane reform (DRM) was described by the global stoichiometric equation $CH_4 + CO_2 \rightarrow 2CO + 2H_2$, where the reaction steps are shown in Table 1. In this model under the reaction conditions (>973 K, 1.0 bar), the cracking of methane (step 1) was considered to be catalytic, the reverse Boudouard reaction was assumed to be heterogeneous non-catalytic (step 2), practically irreversible, while the reverse reaction of water gas-shift (step 3) was qualified as homogeneous.

Table 1. Steps of the reaction for dry methane reform DRM [5].

Step (*i*)	Chemical Equation	Reaction
1	$CH_4 \rightarrow C + 2H_2$	Methane cracking
2	$C + CO_2 \rightarrow 2CO$	Boudouard reverse reaction
3	$CO_2 + H_2 \rightarrow CO + H_2O$	Reverse water gas shift reaction

The evaluations carried out based on the steps evidenced experimentally, used the corresponding reaction rates thus expressed:

$$r_1 = \frac{k_1 K_{CH_4} C_{CH_4}}{1 + K_{CH_4} C_{CH_4}} \tag{5}$$

$$r_2 = k_3 C_{CO_2} \tag{6}$$

$$r_3 = k_3 \left(C_{CO_2} C_{H_2} - \frac{C_{CO} C_{H_2O}}{K_{eq}} \right) \tag{7}$$

The methane autothermal reform (ATRM) occured in the presence of oxygen and water vapor involving steps that formed the steam reform and oxidation of methane. After partial oxidation with oxygen, the process was qualified as an autothermal reform due to the presence of water [15–17]. In the operating conditions practiced (1023 K, 1.0 bar), based on the proposed mechanisms [18], the steps listed in Table 2 were adopted and evaluated for the purposes of the process kinetics.

Table 2. Reaction steps of the autothermal reform of methane ATRM [6].

Step (*i*)	Chemical Equation	Reaction
1	$CH_4 + 1/2O_2 \rightarrow CO + 2H_2$	Partial oxidation of methane
2	$CH_4 + 2H_2O \rightarrow CO_2 + 4H_2$	Steam reforming of methane
3	$CO_2 + H_2 \rightarrow CO + H_2O$	Reverse reaction WGS
4	$CH_4 \rightarrow C + 2H_2$	Methane cracking
5	$C + CO_2 \rightarrow 2CO$	Boudouard reverse reaction
6	$C + O_2 \rightarrow CO_2$	Carbon gasification

The corresponding reaction rates proposed and to be included in the reactor's balance equations were expressed as:

$$r_1 = \left[\frac{k_1 K_{CH4} C_{CH4} (K_{O2} C_{O2})^2}{\left(1 + K_{CH4} C_{CH4} + (K_{O2} C_{O2})^2\right)^2} \right] \tag{8}$$

$$r_2 = \left[\frac{k_2 (C_{CH4} C^2_{H2O}) C^{-3.5}_{H2}}{\left(1 + K_{CH4} C_{CH4} + K_{H2O} C_{H2O} C^{-1}_{H2}\right)^2} \right] \tag{9}$$

$$r_3 = k_3 C_{H2} C_{CO2} \tag{10}$$

$$r_4 = \left[\frac{k_4 K_{CH4} C_{CH4}}{1 + K_{CH4} C_{CH4}} \right] \tag{11}$$

$$r_5 = k_5 C_{CO2} \tag{12}$$

$$r_6 = k_6 C_{O2} \tag{13}$$

Combined methane reform (CRM) is a process that combines dry and steam reforms and oxidation of methane [19–21]. A set of reaction steps based on experimental evidence was proposed [6]. Table 3 lists the reaction steps.

Table 3. Reaction steps of the combined methane reform CRM [7].

Step (*i*)	Chemical Equation	Reaction
1	$CH_4 + 5/8\,O_2 \leftrightarrow CO + 7/4\,H_2 + \frac{1}{4}H_2O$	Partial oxidation of methane
2	$CH_4 \rightarrow C + 2H_2$	Methane cracking
3	$CO \rightarrow 1/2C + 1/2CO_2$	Boudouard reaction
4	$CO_2 + H_2 \rightarrow CO + H_2O$	Reverse reaction of WGS

The reaction rates of the combined reform of methane were expressed for the purpose of quantifying the process kinetics as:

$$r_1 = \left[\frac{k_1 K_{CH4} C_{CH4} K_{O2} C_{O2}}{(1 + K_{CH4} C_{CH4} + K_{O2} C_{O2})^2} \right] \tag{14}$$

$$r_2 = \left[\frac{k_2 K_{CH4} C_{CH4}}{1 + K_{CH4} C_{CH4}} \right] \tag{15}$$

$$r_3 = k_3 C^2_{CO} \tag{16}$$

$$r_4 = k_4 \left(C_{CO_2} C_{H_2} - \frac{C_{CO} C_{H_2O}}{K_{eq}} \right) \tag{17}$$

3.2. Modeling of the Fixed Bed Reactor

The model developed to represent the behavior of the process based on the mass balance equations of the components ($J = CH_4$, CO_2, CO, H_2, H_2O) was of the heterogeneous one-dimensional type, considering axial dispersion and mass transfer effects (Equation (18)).

$$\varepsilon D_{ax} \frac{\partial^2 C_J}{\partial Z^2} - u \frac{\partial C_J}{\partial Z} - (1 - \varepsilon)\rho_{cat} R_J = \varepsilon \frac{\partial C_J}{\partial t} \tag{18}$$

The partial differential equations formulated for the components involved in the different reform processes admitted the initial condition: t = 0, $\forall z\; C_J(0) = 0$ and the following boundary conditions:

$$z = 0,\; \forall t\; C_J(0^-) = \frac{-D_{ax}}{U_0}\left(\frac{\partial C_J}{\partial Z}\right) + C_J(0^+);\; Z = L,\; \forall t\; \frac{\partial C_J}{\partial Z} = 0 \tag{19}$$

Dax is the axial dispersion coefficient of the gas mixture, estimated by the Ruthven correlation (1984) [22], proposed as $D_{ax} = \gamma_1 D_{mJ} + 2\gamma_2 R_p u$, with $u = U_0 \varepsilon^{-1}$, and the tortuosity term, γ_1, is a function of the porosity of the bed (ε). D_{mJ} is the molecular diffusion coefficient of each component and R_p the radius of the catalyst particle ($d_p = 2R_p$, particle diameter).

For the application of the proposed model, especially for the quantifications of the apparent reaction rates (r_{Jap}) terms, possibilities for the occurrence of different kinetic regimes of the catalyst's functioning were considered, involving surface reaction (r_J) and the internal and external mass transfer of the catalyst. Thus, to express the apparent reaction rate, the effectiveness factor η_J ($r_{Jap} = \eta_J r_J$) was quantified according to previous evaluations based on the Weisz criterion (modified Thiele's modulus ($\Phi_J = [r_{Jap} L^2 / De_J C_J]$, $L = d_p/6$)) and the fraction of external resistance ($fe = r_{Jap} L / k_{me} C_J$) [23], where De_J and k_{me} are the internal effective diffusivity and the external mass transfer coefficient, respectively.

4. Results and Discussion

Based on our experimental kinetic operational data of each process ([5–7]) obtained as described in Section 2.1, the validate reaction rate expressions for each component in each process are presented including the kinetic parameters.

The evaluations of the alternative reform processes (DRM, ATRM, CRM) via simulations of their operations in the fixed bed reactor were initially developed for each of the reform processes in operation in the fixed bed reactor, representing the concentrations and the reactants and products by evolutions in different positions on the fixed bed and by profiles at different times of observation. In the sequence, oriented by the comparative evaluation, simulations were carried out on the same experimental bases, focusing on the concentrations of H_2 and CO products, which were represented and compared for the three reform processes.

The experimental data of the processes, which were given by the simulations through the evaluated reaction rates, came from the nickel catalyst (Ni(4.8 wt.%)/γ-Al$_2$O$_3$), which is characterized by the composition (XRD, Figure 1): γ-Al$_2$O$_3$ (2θ 19.4°, 31.9°, 37.6°, 39.5°, 45.9°, 60.9°, 67.0°), Ni (2θ 44.4°, 51.7°, 76.3°, 92.9°, 98.6°), NiO (2θ 37.2°, 62.9°, 43.30°, 62.9°, 75.4°, 79.4°, 95.0°), the spinel NiAl$_2$O$_4$ (2θ 19.1°, 31.4°, 45.0°, 59.7°) [24,25], by the textural characteristics (BET–N$_2$), specific surface area, Sp$_{\gamma\text{-Al2O3}}$ = 174 m^2 g^{-1} and Sp $_{Ni/\gamma\text{-Al2O3}}$ = 165 m^2 g^{-1}), and pore volume, Vp$_{\gamma\text{-Al2O3}}$ = 0.71 cm^3 g^{-1} e Vp$_{Ni/\gamma\text{-Al2O3}}$ = 0.65 cm^3 g^{-1}.
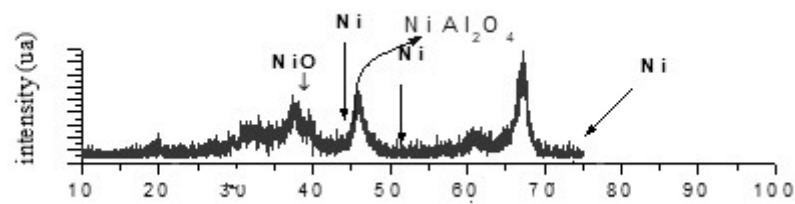
Figure 1. X-ray diffraction (XRD) analysis of the nickel catalyst supported on gamma alumina (Ni (4.82 wt.%)/γ-Al$_2$O$_3$).

In the present development, using the mathematical models as described in Section 2. (Materials and Methods), the operational performance of the processes in the fixed bed reactor was simulated under the conditions listed in Tables 4 and 5.

Table 4. Characteristics of the catalytic system and operating conditions.

Cat. Bed	Operation	Parameters
Ni (4.87%wt.)/γ-Al$_2$O$_3$	U_o, 0.66 m s^{-1}	D_{ax}, 7.89 × 10^{-4} m^2 s^{-1}
ε, 0.67	1023 K	
ρ_{cat}, 2300 kg m^{-3}	1.0 bar	
d_{pt}, 2.0 × 10^{-3} m		
w$_{cat}$, 10.4 g		

Table 5. Composition of the reactor feed in the operation of the reform processes.

Reactant	DRM (mol m^{-3})	ATRM (mol m^{-3})	CRM (mol m^{-3})
CH$_4$	11.4	20	43
CO$_2$	16.0	-	25
O$_2$	-	4.0	1.7
H$_2$O	-	12	12

In terms of hydrogen and carbon monoxide productions, comparisons were made taking into account the concentration evolutions (C_J vs. t) and concentration profiles (C_J vs. z). The formulated mass balance equation (Equation (18)) for the components of each reform, performed in the fixed bed reactor was expressed including the respective general reaction rate (R_J, Equation (20)), considering the rates of reaction steps (r_J) assumed in the kinetic evaluation of the processes.

$$R_J = \sum_J r_{Jap} = \sum_J \eta_J r_J \tag{20}$$

where $r_J = \nu_{iJ}\, r_i$, *and* ν_{iJ} is the stoichiometric coefficient of the J component in reaction step i.

In the processes involving the direct or reverse reaction step of water gas shift, the equilibrium constant (K_{eq}) was employed as a function of the temperature expressed as follows:

$$K_{eq} = \exp\left(-6.31 \times 10^{-2} - 1.86 \times 10^{-7} \ln(T) + 2.11 \times 10^{-4}T + \frac{9.37 \times 10^{-1}}{T} - \frac{5.44 \times 10^{-6}(T - 298.15)}{T^2}\right) \tag{21}$$

For each reform process, the specific reaction rates evaluated under the operating conditions and the global reaction rates (R_J) for the CH$_4$, H$_2$ and CO components are listed in Tables 6–8.

Table 6. Reaction rates of the dry reform of methane. Conditions: Ni (4.82 wt.%)/γ-Al$_2$O$_3$,1023 K, 1.0 bar [5].

J	Consumption	Production	R_J
CH$_4$	Step 1 k$_1$ = 6.79 × 10^{-4} mol kg^{-1}s^{-1}	-	r_1
CO	Step 2 k$_2$ = 9.89 × 10^{-6} (m^3)^2 mol^{-1}kg^{-1}s^{-1}	Step 1 k$_1$ = 6.79 × 10^{-4} mol kg^{-1}s^{-1}	$2r_1 + r_3$
H$_2$	-	Steps 2, 3 k$_2$ = 9.89 × 10^{-6} (m^3)^2 mol^{-1}kg^{-1}s^{-1} k$_3$ = 3.94 × 10^{-4} m^3 kg^{-1}s^{-1}	$2r_2 + r_3$

Table 7. Reaction rates of the autothermal reform of methane. Conditions: Ni(4.8 wt.%)/γ-Al$_2$O$_3$, 1023 K, 1.0 bar [6].

J	Consumption	Production	R_J
CH$_4$	Steps 1, 2, 4 k$_1$ = 1.31 × 10^{-1} mol/kg s k$_2$ = 8.30 × 10^{-2} (m^3)^2/kg s mol k$_4$ = 1.04 × 10^{-1} m^3/kg s	-	$-r_1 - r_2 - r_4$
CO	Step 3 k$_3$ = 4.11 × 10^{-5} m^3/kg s	Steps 1, 5 k$_1$ = 1.31 × 10^{-1} mol/kg.s k$_5$ = 9.41 × 10^{-8} m^3/kg s	$2r_1 - r_3 + r_5$
H$_2$	Step 3 k$_3$ = 4.11 × 10^{-5} m^3/kg s	Steps 1, 2, 3, 4 k$_1$ = 1.31 × 10^{-1} mol/kg s k$_2$ = 8.30 × 10^{-2} (m^3)^2/kg s mol k$_4$ = 1.04 × 10^{-1} m^3/kg s	$2r_1 + 4r_2 - r_3 + 2r_4$

Table 8. Reaction rates of the combined reform of methane. Conditions: Ni (4.82 wt.%)/γ-Al$_2$O$_3$, 1023 K, 1.0 bar [7].

J	Consumption	Production	R_J
CH$_4$	Step 1 k$_1$ = 6.79 × 10^{-4} mol kg^{-1}s^{-1}		$-r_1 - r_2$
CO	Step 2 k$_2$ = 9.89 × 10^{-6} (m^3)^2 mol^{-1}kg^{-1}s^{-1}	Step 1 k$_1$ = 6.79 × 10^{-4} mol kg^{-1}s^{-1}	$r_1 + r_3 + 2r_5$
H$_2$	-	Steps 2, 3 k$_2$ = 9.89 × 10^{-6} (m^3)^2 mol^{-1}kg^{-1}s^{-1} k$_3$ = 3.94 × 10^{-4} m^3 kg^{-1}s^{-1}	$(7/4)r_1 + 2r_2 - r_4$

Under the practiced conditions and according to the reaction speeds of methane consumption, the criteria (*phi'*, *fe*) were calculated to quantify the evaluation of the kinetic regimes of mass transfer in relation to the reaction kinetics. Weisz's modulus (modified Thiele's modulus) *phi'* and the external resistance fraction *fe* were estimated in the following ranges, *phi'*$_{CH4}$ = [0.22 − 8.35] × 10^{-4} close to zero, and *fe*$_{CH4}$ = [1.07 − 1.43] × 10^{-2} less than 0.02. Thus, the low limitations imposed by mass transfer were characterized, so that $\eta_J \rightarrow 1$, $r_{Jap} \approx r_J$. Figure 2 shows the evolution of the component concentrations (CH$_4$, CO$_2$, H$_2$O, O$_2$, H$_2$, CO) of the alternative reforms DRM, ATRM, and CRM, characterized for the initial times of each operation.
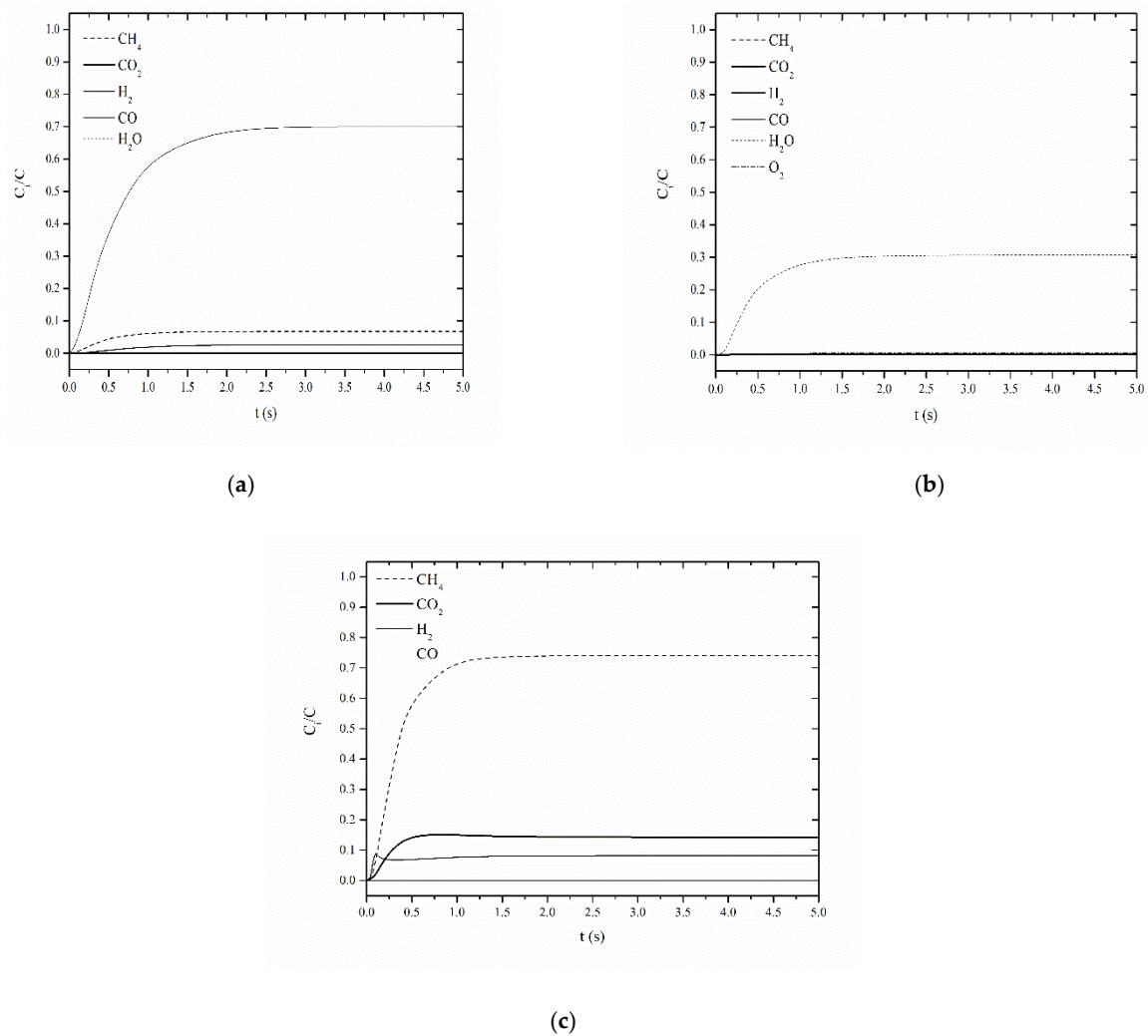
(a)

(b)

(c)

Figure 2. Alternative methane reform processes. Evolution of concentrations. (**a**) DRM, (**b**) ATRM, (**c**) CRM. Conditions: Cat. Ni (4.82 wt.%)/γ-Al$_2$O$_3$, 1023 K, 1.0 bar.

The concentration evolutions were more advanced for the feed reagents and then for product evolutions. In general, it was indicated for the three reforms that after approximately three seconds the steady state was reached. The short times for the operation to become stationary were due to the small bed size and the relatively high flow of gas flowing through it.

In Figure 3, for comparison purposes, the concentration profiles of hydrogen and carbon monoxide (C_{H2}, C_{CO}) in the three alternative reforms are represented. The hydrogen concentration profiles for the three reforms were similar and increasing, and showed levels that varied according to bed positions, from the inlet to the outlet of the reactor. In the positions close to the reactor inlet (0.1 L), the hydrogen production was higher in the DRM operation, with a concentration approximately 50% higher than that obtained in the ATRM, and much higher than the concentration achieved in the CRM. However, at the outlet of the reactor that represented the production of the system, the level of hydrogen concentration obtained in the operation of the CRM was 75% higher than that of the DRM, while in the ATRM the concentration was lower, about twice lower.
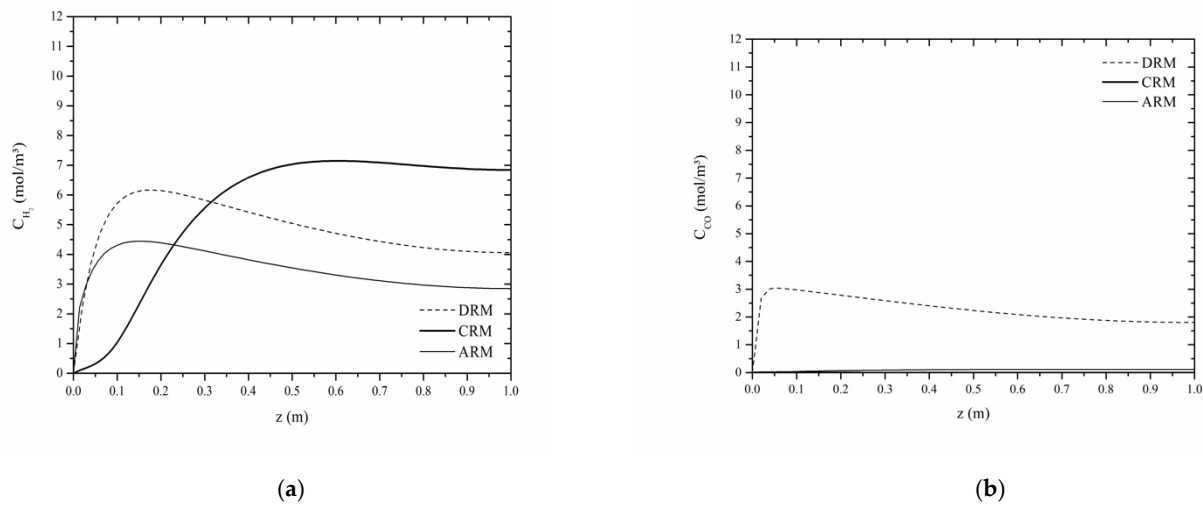
(a)   **(b)**

Figure 3. Comparison of alternative methane reform processes. Concentration profiles. (**a**) H_2, (**b**) CO. Conditions: Cat. Ni (4.82 wt.%)/γ-alumina, 1023 K, 1.0 bar.

The alternative reforms evaluated according to the kinetics of their reaction steps (i = 1, 2, 3, etc.) that formed the mechanism of each process reflected the evolutionary characteristics of the productions. To express them, using the specific rates of the reaction steps related to each product (k_{iJ}), it was possible to calculate the kinetic selectivities defined as $S_J = \sum_i \nu_{iJ} k_{iJ} [\sum_i k_i]^{-1}$, where J is a product present in the reaction step i, and ν_{iJ} its stoichimetric coefficient for comparative evaluation purposes, S_J is calculated for H_2 and CO according to Equations (22)–(24), denominated $S_{J\text{-}DRM}$, $S_{J\text{-}ATRM}$ and $S_{J\text{-}CRM}$, respectively.

$$S_{H2-DRM} = 10^2 (2k_1 - k_3)_{DRM} \left[\sum_i k_{i-DRM} \right]^{-1}, \; S_{CO-DRM} = 10^2 (k_2 + 2k_3)_{DRM} \left[\sum_i k_{i-DRM} \right]^{-1} \tag{22}$$

$$S_{H2-ATRM} = 10^2 (2k_1 + 4k_2 - k_3 + 2k_4)_{ATRM} \left[\sum_i k_{i-ATRM} \right]^{-1}, \; S_{CO-ATRM} = 10^2 (k_1 - 2k_3 + k_4)_{ATRM} \left[\sum_i k_{i-ATRM} \right]^{-1} \tag{23}$$

$$S_{H2-CRM} = 10^2 (7/4 k_1 + 2k_2 - k_4)_{CRM} \left[\sum_i k_{i-CRM} \right]^{-1}, \; S_{CO-CRM} = 10^2 (k_1 - 2k_3 + k_4)_{CRM} \left[\sum_i k_{i-CRM} \right]^{-1} \tag{24}$$

In Table 9, the orders of magnitude of the kinetic selectivities S_{H2} and S_{CO} calculated through the Equations (22)–(24) are listed.

Table 9. Kinetic selectivities of products (H_2, CO).

Reform	Kinetic Selectivities S_{ip} (%, $i = H_2, CO$)	
Product	H_2	CO
DRM	13.3	59.2
ATRM	31.6	28.3
CRM	86.1	5.1

The kinetic selectivities indicated the following highlights for the CRM process, with $S_{H2\text{-}CRM}$ = 86.1%, and for the DRM process, with $S_{CO\text{-}DRM}$ = 59.2%, which characterized the process guidelines for the selective production of hydrogen and carbon monoxide. Hydrogen productions, considering the reaction steps for consumption in each reform process, had their specific rates in the following orders of magnitude: 10^{-4} DRM, 10^{-1} ATRM, and 10^2 CRM, involving, respectively, one-step, three-step, and two-step reactions. Such checks showed compliance with the highest levels of evolution and profiles obtained in the operations of CRM. On the other hand, the production of carbon monoxide occurred more quickly and at higher levels in DRM operations, where the process produced it through two reaction steps.

The prospects for operating selective synthesis gas and/or hydrogen productions by methane reforming can be based on the simulations obtained for a fixed bed reactor that converge to the MRC choice. To be viable, this choice must resort to the use of a low-cost Ni catalyst, which operates in a chemical kinetic regime and with minimal loss of activity.

In this sense, it is intended to operate with a fixed bed reactor structured in monolith, when the Ni phase is dispersed on the walls of the multichannel system. Thus, the system will work in a chemical kinetic regime and with low pressure drops, allowing high processing flows.

5. Conclusions

Using experimental kinetic bases, predictions were made for methane reform operations, characterized as dry reform (DRM), autothermal reform (ATRM), and combined reform (CRM), constituting alternatives to steam reform of methane. Simulations were developed using a heterogeneous model for operations in a fixed bed reactor compacted with the catalyst Ni (4.8 wt.%)/γ-Al$_2$O$_3$ at 1023 K and 1.0 bar, considering the reactor fed with CH_4/CO_2 in DRM, $CH_4/H_2O/O_2$ in ATRM, and $CH_4/CO_2/H_2O/O_2$ in CRM.

The simulations of the operations were expressed in terms of the concentrations of the components as evolutions, in different positions of the fixed bed, and as profiles, for various times of observation. The predictions allow the following behaviors to be indicated for processes:

- The evolution of the concentration of reagents and products increase and are similar between them, with the reagents evolving in the reactor earlier, and the products afterwards;
- The reagent profiles decrease, while the product profiles increase, reaching higher levels of concentration in the outlet sector of the reactor;
- Carbon yields can be predicted at low levels, where the reaction steps involving its production are compensated by its consumption, according to interactions with O_2, CO_2 and H_2O.

The predicted behaviors serve as a basis for the comparative evaluations of the different reforms of methane, which were elaborated by analyzing the profiles of methane, hydrogen and carbon monoxide, establishing the following conclusions:

- Methane is always consumed in the operations of the three reforms; this consumption occurs at the CRM via three reaction steps, with a predominance of the order of magnitude 10^2 of the specific reaction rates compared to the orders of 10^{-4} and 10^{-1} in the operations of the DRM and ARM reforms;
- Hydrogen production, considering the steps that involve consumption in each reform process, have their specific rates in the following orders of magnitude: 10^{-4} DRM, 10^{-1} RAM, and 10^2 RCM, considering, respectively, one step, three steps, and two reaction steps;
- The production of carbon monoxide occurs more quickly and at higher levels in DRM operations where its conversion is not verified, and the referred production occurs through two reaction steps.

The comparisons according to the performance of the alternative reforms were made through the kinetic selectivities of H_2 and CO. Thus, in the course of operations in the fixed bed reactor, the CRM and DRM reforms highlight, respectively, a hydrogen selectivity of 86.1% and a carbon monoxide selectivity of 59.2%.

Author Contributions: Conceptualization and methodology, A.K. and M.A.M.S.; software and validation, D.C.S.S. formal analysis and investigation, A.K. and C.A.M.A.; revision and editing C.A.M.A. All authors read and agreed with the published version of the manuscript.

Institutional Review Board Statement: Not applicable.

References

1. Armor, J.N.; Martenak, D.J. Studying carbon formation at elevated pressure. *Appl. Catal. A Gen.* **2001**, *206*, 231–236. [CrossRef]
2. Rostrupnielsen, J.; Hansen, J.H.H.T.A.B. CO$_2$-Reforming of Methane over Transition Metals. *J. Catal.* **1993**, *144*, 38–49. [CrossRef]
3. Tomishige, K.; Yamazaki, O.; Chen, Y.; Yokoyama, K.; Li, X.; Fujimoto, K. Development of ultra-stable Ni catalysts for CO$_2$ reforming of methane. *Catal. Today* **1998**, *45*, 35–39. [CrossRef]
4. Takenaka, S.; Ogihara, H.; Yamanaka, I.; Otsuka, K. Decomposition of methane over supported-Ni catalysts: Effects of the supports on the catalytic lifetime. *Appl. Catal. A Gen.* **2001**, *217*, 101–110. [CrossRef]
5. Abreu, C.A.M.; Santos, D.A.; Pacífico, J.A.; Filho, N.M.L. Kinetic Evaluation of Methane−Carbon Dioxide Reforming Process Based on the Reaction Steps. *Ind. Eng. Chem. Res.* **2008**, *47*, 4617–4622. [CrossRef]
6. Souza, A.E.A.M.; Maciel, L.J.L.; Cavalcanti-Filho, V.O.; Filho, N.M.L.; Abreu, C.A.M. Kinetic-Operational Mechanism to Autothermal Reforming of Methane. *Ind. Eng. Chem. Res.* **2011**, *50*, 2585–2599. [CrossRef]
7. Maciel, L.J.L.; Souza, A.E.A.M.; Vasconcelos, S.M.; Knoechelmann, A.; Abreu, C.A.M. Dry reforming and partial oxidation of natural gas to syngas production. *Stud. Surf. Sci. Catal.* **2007**, *167*, 469–474.
8. Singh, R.; Dhir, A.; Mohapatra, S.K.; Mahla, S.K. Dry reforming of methane using various catalysts in the process. *Biomass Convers. Biorefinery* **2020**, *10*, 567–587. [CrossRef]
9. Song, Y.; Ozdemir, E.; Ramesh, S.; Adishev, A.; Subramanian, S.; Harale, A.; Albuali, M.; Fadhel, B.A.; Jamal, A.; Moon, D.; et al. Dry reforming of methane by stable Ni–Mo nanocatalysts on single-crystalline MgO. *Science* **2020**, *367*, 777–781. [CrossRef] [PubMed]
10. Luneau, M.; Gianotti, E.; Guilhaume, N.; Landrivon, E.; Meunier, F.C.; Mirodatos, C.; Schuurman, Y. Experiments and Modeling of Methane Autothermal Reforming over Structured Ni–Rh-Based Si-SiC Foam Catalysts. *Ind. Eng. Chem. Res.* **2017**, *56*, 13165–13174. [CrossRef]
11. Chen, J.; Li, L. Mechanism of the autothermal reforming reaction of methane on Pt(1 1 1) surfaces: A density functional theory study. *Appl. Surf. Sci.* **2021**, *539*, 148288. [CrossRef]
12. Lino, A.V.P.; Assaf, E.M.; Assaf, J.M. Adjusting Process Variables in Methane Tri-reforming to Achieve Suitable Syngas Quality and Low Coke Deposition. *Energy Fuels* **2020**, *34*, 16522–16531. [CrossRef]
13. Lino, A.V.P.; Calderon, Y.N.C.; Mastelaro, V.R.; Assaf, E.M.; Assaf, J.M. Syngas for Fischer-Tropsch synthesis by methane tri-reforming using nickel supported on MgAl$_2$O$_4$ promoted with Zr, Ce and Ce-Zr. *Appl. Surf. Sci.* **2019**, *481*, 747–760. [CrossRef]
14. Chen, L.; Gangadharan, P.; Lou, H.H. Sustainability assessment of combined steam and dry reforming versus tri-reforming of methane for syngas production. *Asia Pac. J. Chem. Eng.* **2018**, *13*, e2168. [CrossRef]
15. Dias, A.C.J.; Assaf, J.M. The advantages of air addition on the methane steam reforming over Ni/γ-Al$_2$O$_3$. *J. Power Sources* **2004**, *137*, 264–268. [CrossRef]
16. Liu, S.; Xiong, G.; Dong, H.; Yang, W. Effect of carbon dioxide on the reaction performance of partial oxidation of methane over a LiLaNiO/γ-Al$_2$O$_3$ catalyst. *Appl. Catal. A Gen.* **2000**, *202*, 141–146. [CrossRef]
17. Larentis, A.L.; de Resende, N.S.; Salim, V.M.M.; Pinto, J.C. Modeling and optimization of the combined carbon dioxide reforming and partial oxidation of natural gas. *Appl. Catal. A Gen.* **2001**, *215*, 211–224. [CrossRef]
18. Lu, Y.; Xue, J.; Yu, C.; Liu, Y.; Shen, S. Mechanistic investigation on the partial oxidation of methane to syngas over a nickel-on-alumina catalyst. *Appl. Catal. A Gen.* **1998**, *174*, 121–128. [CrossRef]
19. Hong-Tao, J.; Hui-Quan, L.; Yi, Z. Tri-reforming of methane to syngas over Ni/Al$_2$O$_3$-Thermal distribution in the catalyst bed. *J. Fuel Chem. Technol.* **2007**, *35*, 72–78.
20. Lee, S.-H.; Cho, W.; Ju, W.-S.; Cho, B.-H.; Lee, Y.-C.; Baek, Y.-S. Tri-reforming of CH4 using CO$_2$ for production of synthesis gas to dimethyl ether. *Catal. Today* **2003**, *87*, 133–137. [CrossRef]
21. Seo, Y.S.; Shirley, A.; Kolaczkowski, S.T. Evaluation of thermodynamically favorable operating conditions for production of hydrogen in three different reforming technologies. *J. Power Sources* **2002**, *108*, 213–225. [CrossRef]
22. Ruthven, D.M. *Principles of Adsorption and Adsorption Process*; John Wiley & Sons: Hoboken, NJ, USA, 1984.
23. Villermaux, J. *Génie de la Reaction Chimique: Conception et Fonctionement des Reactors*; Technique et Documentation (Lavoisier), 2ª triage: Paris, France, 1982.
24. Valentini, A.; Carreno, N.L.V.; Leite, E.R.; Goncalves, R.F.; Soledade, L.E.B.; Maniette, Y.; Longo, E.; Probst, L.F.D. Improved activity and stability of Ce-promoted Ni/gamma-Al$_2$O$_3$ catalysts for carbon dioxide reforming of methane. *Lat. Am. Appl. Res.* **2004**, *34*, 165–172.
25. Maluf, S.S.; Assaf, E.M.; Assaf, J.M. Catalisadores Ni/Al$_2$O$_3$ promovidos com molibdênio para a reação de reforma a vapor de metano. *Quím. Nova* **2003**, *26*, 181–187. [CrossRef]